PPPL-1928

UC20-A,B,F

I-6038

PPPL-1928
Dr. 935

MASTER

AUXILIARY HEATING RESULTS FROM PDX AND PLT

By

S.L. Davis, PDX and PLT Groups

SEPTEMBER 1982

PLASMA PHYSICS LABORATORY

PRINCETON UNIVERSITY
PRINCETON, NEW JERSEY

PREPARED FOR THE U.S. DEPARTMENT OF ENERGY,
UNDER CONTRACT DE-AC02-76-CHO-3073.

NOTICE

Printed in the United States of America.

Available from:

National Technical Information Service
U. S. Department of Commerce
5285 Port Royal Road
Springfield, Virginia 22151

Price: Printed Copy $ * ; Microfische $3.50

*PAGES	NTIS Selling Price
1-25	$5.00
26-50	$6.50
51-75	$8.00
76-100	$9.50
101-125	$11.00
126-150	$12.50
151-175	$14.00
176-200	$15.50
201-225	$17.00
226-250	$18.50
251-275	$20.00
276-300	$21.50
301-325	$23.00
326-350	$24.50
351-375	$26.00
376-400	$27.50
401-425	$29.00
426-450	$30.50
451-475	$32.00
476-500	$33.50
500-525	$35.00
526-550	$36.50
551-575	$38.00
576-600	$39.50

For documents over 600 pages, add $1.50 for each additional 25 page increment.

PPPL--1928

DE83 001393

Ninth Annual Conference on Plasma Physics
30 June - 2 July, 1982, Oxford

AUXILIARY HEATING RESULTS FROM PDX AND PLT

S.L. Davis, PDX and PLT Groups

Princeton University, Plasma Physics Laboratory
Princeton, New Jersey 08544 USA

Abstract —— Auxiliary heating experiments are continuing on both PLT and PDX. PLT has increased the available ICRF power delivered to the plasma to 3 MW for the 42 MHz system and to 1.6 MW for the 25 MHz system. Deuteron and electron heating are observed in the minority ^{3}He ($T_d \sim 2.8$ keV, $T_e \sim 2.2$ keV) and H ($T_d \sim 2$ keV, $T_e \sim 2.5$ keV) heating regimes. In addition, ion heating has been observed in the second harmonic regime ($T_{eff} = 2/3 \langle E_h \rangle = 3.3$ keV).

On PDX, the evaluation of the effectiveness of perpendicular injection has continued with available beam powers of 7.2 MW for deuterium beams and 5.5 MW for hydrogen beams. Peak ion temperatures of ~ 6 keV have been achieved for 500 kA plasmas, indicating that ion heating efficiencies can be obtained with perpendicular injection similar to what was obtained on PLT with tangential injection. At lower plasma currents, the ion heating efficiency is reduced. Neutral beam studies on PDX have now been conducted over a wider range of parameters. Results from these studies will be discussed.

Recent auxiliary heating of low q ($\lesssim 2$) discharges on both PLT and PDX have resulted in substantial plasma β in both machines. PDX has used an absorbed beam power of 5.0 MW at a field of 1.0T with $q_\phi = 1.8$ to obtain a beta of 3.2% measured magnetically. PLT has used combined beam and ICRF heating in the minority mode to obtain a toroidal β in the range of 1.6 to 2.2% with ~ 3 MW total power, 1.7 T field, and $q_\phi \simeq 2.2$.

On PLT, 800 MHz lower hybrid waves have been launched at powers up to 600 kW. At low densities ($< 10^{13}$ cm^{-3}), experiments have demonstrated both current drive ($\bar{n}_e I_p/P_{LH} \sim 6 \times 10^{12}$ A/W cm^3) with $V_{loop} \simeq 0$ for times up to 3.5 seconds. Experiments at higher densities have produced hot ion tails, but so far have shown only inefficient bulk ion heating.

1. INTRODUCTION

The Princeton Large Torus (PLT) and Poloidal Divertor Experiment (PDX) are both large tokamaks primarily devoted to the study of techniques for plasma heating, current drive, and of confinement scaling with auxiliary heating. The PDX machine typically runs one second discharges with $a \leq 44$ cm, $R_o \simeq 143$ cm, $I_p \lesssim 500$ kA, and $B_T < 2.4$ T. The PDX experiments (Section 2) have focused on the study of neutral beam heating of circular and diverted plasmas, with more recent efforts directed toward the study of low q, high β plasmas by running at low toroidal fields ($B_T \lesssim 1.2$ T).

The PLT machine operates with circular plasmas having normally a = 40 cm, $R_o = 132$ cm, $I_p \lesssim 550$ kA, and $B_T \lesssim 3.2$ T. The PLT experiments have focused on the study of ICRF and ICRF plus neutral beam heating (Section 3) as well as lower hybrid heating and current drive (Section 4).

2. PDX NEUTRAL BEAM HEATING RESULTS

The PDX neutral injection system, developed through a joint PPPL and ORNL program, quickly reached its design parameters of 8 MW of D° and 6 MW of H° from nominally 50 keV ion sources. With duct losses subtracted, input powers to the PDX vacuum vessel of 7.2 MW of D° and 5.5 MW of H° have been achieved. The beams are injected nearly perpendicular (14° from $\perp$ at R_o = 142 cm).

Ion temperatures during neutral beam heating experiments have been measured using two techniques. Passive charge exchange ion temperature measurements are made using a four analyzer system each with ten energy channels, which allows complete temporal and four point radial profile measurements. The charge exchange system is further equipped with a diagnostic neutral beam to provide localized measurements of the ion

temperature. The second technique uses a crystal spectrometer to observe Doppler broadening of a Ti XXI K_α line at 2.61 Å to yield central impurity temperatures. The measurements are compared in Fig. 1. Ion temperature profiles are also measured from ultraviolet doppler broadening of forbidden line transistions from a number of artificially injected impurities (Suckewer 1980).

A plot of T_i versus $P_{abs}/\bar{n}_e$ is shown in Fig. 2. The quantity P_{abs} is the absorbed beam power (injected beam power minus shinethrough), $\bar{n}_e$ is the line average density, and T_i is the ion temperature measured by passive charge exchange. The data indicate a clear improvement of ion heating efficiency with increasing plasma current, but due to the scatter of the data no simple scaling law can be extracted. Ion temperatures of ~ 6 keV have been achieved in high current (I_p = 500 kA), high field (2.2T) discharges with absorbed beam powers of ~ 4 MW. The ion heating efficiencies, $\eta_i \equiv \bar{n}_e \Delta T_i/P_{abs}$, obtained in PDX are comparable to those obtained with tangential injection on PLT (Stodiek 1980, Goldston 1981). Transport analysis code studies indicate that η_i is a relatively good measure of ion heating efficiency and ion energy confinement (Hawryluk 1982). With a fixed ion thermal transport model, η_i is found not to depend strongly on $n_e(r)$, $T_e(r)$ or Z_{eff} in the density range $1 - 4 \times 10^{13}$ cm^{-3}. The ion transport for high power beam heated, 500 kA discharges on PDX can be accurately modeled using neoclassical conduction (Chang 1982), classical ion-electron coupling, and phenomenological convective losses (5/2 kTΓ). In lower current discharges the ion thermal conduction is found to be enhanced over neoclassical. Although there is some variability in both the PDX and PLT heating efficiencies, it is clear that under similar high field, high current conditions tangential and perpendicular injection can yield similar ion heating results.

Electron temperature and density profiles on PDX have been measured using a 56 point Thomson scattering system with the profile taken in the horizontal plane along the major radius. With neutral beam injection, the electron energy content is found to rise with increasing beam power. At power levels up to about 2 MW and at 22 kG, typical electron heating of 0.5 eV/kW is observed, which is comparable to the electron heating observed on PLT with similar powers. At higher absorbed beam powers (up to 5.5 MW) $\Delta T_e/P_{abs}$ was reduced. This effect appears to be due to the increase in line average density which occurs with increasing beam power. In general, τ_{Ee} is found not to increase linearly with $\bar{n}_e$ on either PLT or PDX with neutral beam injection, and thus a density rise reduces $\Delta T_e(o)$ (Goldston 1982). Central radiation on PDX is typically found to be less than 10% of the total central input power, as measured by the bolometer and substantiated by the soft X-ray and ultraviolet measurements. Transport analysis of the electron energy confinement in beam heated ($P_b \geq 1.5$ MW, $D^o \rightarrow H^+$) 500 kA circular discharges indicates that the global energy confinement time for the thermal plasma was about 23 ms, independent of beam power (Hawryluk 1982).

Magnetic equilibrium measurements of $\Lambda = \ell_i/2 + \beta_\theta$ have been used to estimate the stored plasma energy. The change in Λ versus beam power for several different currents is shown in Fig. 3. The internal inductance term can be estimated from a simple model which depends only the value of q at the limiter.† The higher power discharges at 200 kA have reached values of β_θ of ~ 2.0 without a clear indication of saturation with beam power as on ISX-B (Swain 1981) or DITE (Lomas 1981). Since the electron energy increases

† In this model we assume $j \propto (1-(r/a)^2)^x$, where $x = q(a)/q(o)-1$. $q(o)$ is taken to be the greater of $q(a)/4$, and 1. The estimated uncertainty in $\ell_i/2$ for this model is ± 15%.

linearly with beam power, the equilibrium measurements imply that the stored energy in the beam and thermal ions also increases roughly linearly with beam power. The magnetic measurements confirm the improvement in confinement with plasma current seen in the ion heating results.

Recent attention on PDX has focused on the production and study of low q, high β discharges at low toroidal fields. The highest toroidal beta, β_T, achieved to date is 3.2%, measured by the diamagnetic signal. This was obtained with an absorbed beam power of 5.0 MW, at 1.0 T and with $q_\psi = 1.7$, assuming that all of the measured plasma current flows within the limiter radius. The value of β_T from the equilibrium analysis was 3.0% for this discharge. The difference may be due to beam anisotropy.

The dependence of β_T on absorbed beam power has been documented for a 1.0 T, 300 kA plasma with $\bar{n}_e = 4 \times 10^{13}$, and $q_\psi = 2.1$ (Fig. 4). The beta values shown here are derived from the equilibrium measurement. The q dependent model for $\ell_i/2$ is assumed. The time evolution of I_p and $\bar{n}_e$ was maintained constant despite the very different injected powers in the various cases. In the OH case, however, while I_p was maintained at 300 kA, $\bar{n}_e$ was $\lesssim 3 \times 10^{13}$ cm^{-3}. Thus, the OH case may not be directly comparable with the others. The data shown in the power scan were taken after 150 msec of beam injection. As is normally the case with high β_T discharges, β_T, I_p, $\bar{n}_e$, and consequently τ_E were increasing at the time the measurements were made. Energy analysis of lower power ($\lesssim$ 2.7 MW) cases with $B_T \lesssim 2\%$, using a Monte Carlo beam code which assumes neoclassical beam ion confinement, have shown good agreement with the magnetically measured beta values. At higher powers and beta values, the energy analysis consistently gives higher values. Figure 5 shows the stored plasma energy determined from the equilibrium measurement assuming isotropic plasma pressure. The data have been restricted to 300 kA

discharges, with B_T = 2.2 T and 1.0 T. The data suggest that the toroidal field has little effect on stored plasma energy in the range 1.0 T - 2.2 T.

Distinctive MHD activity (Figs. 6 and 7), has been observed during high β_T discharges on the Mirnov coils, on the soft X-ray wave detector array, on a fast neutron detector, and on the charge exchange signals. The Mirnov and X-ray signals may be similar to what has been observed on JFT-2 (Yamamoto 1981) and ISX-B (Dunlap 1982). This activity may also be similar to the "fast ion disruptions" which were observed on PLT during some high temperature runs (PPPL 1981). On PDX, the soft X-ray wave detector array indicates the presence of a m = n = 1 structure which grows and dies in short bursts (on a $\lesssim$ 1 msec times scale), with a period between bursts of generally 2-5 msecs. Each burst correlates with a packet of oscillations on the Mirnov coils. The period between bursts appears to become shorter with lower toroidal field. On a faster time scale, the internal structure at B_t = 1.0 T is seen to consist predominately of a packet of $\sim$ 11 kHz oscillations, although at the onset of the bursts, frequencies up to 150 kHz have been observed. The 11 kHz frequency may correspond to toroidal rotation of the m = n = 1 structure at a velocity equal to the measured plasma rotation velocity at the q = 1 surface [$(0.5 - 1) \times 10^7$ cm/sec]. The structure seen on the Mirnov coils is identical in frequency and is phase locked to the mode observed on the ultra soft X-ray signal (Fig. 6). The charge exchange signals (Fig. 7) show large spikes of enhanced flux from thermal energies up to $\sim$ 80 keV, which also correlate with the bursts. The enhanced flux is strongly peaked in the perpendicular direction, especially at energies above the injection energy, and at energies around 10 - 12 keV (Fig. 8). The internal 11 kHz structure of the individual fishbones can also be seen on the charge exchange systems. They are observed to be phase locked to the X-ray signals such that the enhanced efflux occurs

when the hot spot of the internal structure is facing the analyzers. In the high β_T discharges at high power, the slowing down spectra of the beam particles show an indication of depletion due to the bursts, but the quantitative effect on the stored beam energy and heating efficiency is as yet unclear. The clearest signs of depletion occur at energies just below the injection energy (35 keV $\leq$ E $\leq$ 50 keV) and at angles close to perpendicular. With $D^0 \rightarrow H^+$ injection, the neutron flux (due predominately to beam-target and beam-beam reactions) shows a rapid ($\sim$ 300 sec) $\sim$ 30% decrease during each burst, which clearly is indicative of the loss of fast ions from the slowing down distribution. The oscillations become stronger with the application of more beam power. With less than two beams, the normal sawtooth oscillations occur, while increasing from two to four beams causes the activity to become more pronounced with the addition of each beam.

3. PLT AUXILIARY HEATING RESULTS

With the addition of two more antennas on PLT, a substantial increase in the power handling capability of the ICRF system has been achieved (Hosea 1982). At 42 MHz the highest power delivered to the plasma has been increased to 3 MW by using six 1/2 turn antennas, while the 25 MHz system has delivered up to 1.6 MW using four of these same antennas. Both ion and electron heating have been observed in the minority ^3He and H heating regimes in deuterium plasmas. In addition, ion heating has been observed in the second harmonic regime.

The highest central deuterium temperature has been reached in the ^3He minority regime with a deuterium plasma at 2.5 T using the 25 MHz system. Figure 9 shows the neutron flux increased by roughly three orders of magnitude with the application of 1.3 MW of ICRF power. The central deuterium

temperature deduced from this flux rose from 0.8 keV to 2.8 keV at a density of $\bar{n}_e \simeq 3.2 \times 10^{13}$ cm^{-3}. This temperature rise is also measured by the mass sensitive charge exchange system. The presence of an energetic ^{3}He tail has been confirmed by the measurement of 14.7 MeV protons from the d(^{3}He, ^{4}He)p reaction as measured by a Si surface barrier detector (Chrien 1981). The proton energy spectra are produced by reacting particles with an average energy in the range 100-400 keV. The central electron temperature in a similar ^{3}He minority experiment was observed to rise from ~ 1 keV to ~ 2.2 keV (Fig. 10) while the density rose from 3 to 3.8 x 10^{13} cm^{-3} with 1.5 MW of ICRF power absorbed. These heating results are found to be consistent with minority heating theory (Hosea 1979) which passes all ICRF power directly to the ^{3}He tail, and then couples this energy to the bulk electrons and deuterons.

In the hydrogen minority case at 2.8 T and 42 MHz, preliminary experiments with power levels up to 2.5 MW have been performed. At power levels of 1.4 MW, ion and electron heating have been documented. With an input power of 1.4 MW for a duration of 300 msec, an increase of two orders of magnitude in the production of neutrons from the majority deuterons was observed. The deduced ion temperature rose from 0.7 to 1.7 keV.

The central ion heating efficiencies are compared in Fig. 11 for the various minority regimes. The fundamental ^{3}He minority case shows the highest ion heating efficiency with η_i = 5-6 x 10^{13} eV/kW cm^3, while the H minority mode shows an ion heating efficiency of η_i = 3-4 x 10^{13} eV/kW cm^3. The minority heating cases shown have been selected to represent the optimal ion heating results observed in these experiments. The higher ion heating efficiency for the ^{3}He case occurs partially because of the lower charge exchange losses for ^{3}He, but also because the ^{3}He couples more strongly to the bulk plasma and therefore gives a larger fraction of its energy to the ions.

The highest absorbed RF powers to date (3.0 MW) have been launched at 42 MHz into a 1.4 T hydrogen plasma. The resulting bulk ion energy distribution produced by second harmonic heating was found to be non-Maxwellian (Fig. 12), in general qualitative agreement with quasi-linear velocity space diffusion theory. Diagnostic neutral beam measurements have been used to show that the passively measured distribution is present in the center of the plasma. The passively measured charge exchange distribution in the second harmonic heating cases has been characterized by an effective temperature defined by

$$T_{eff} \equiv \frac{2}{3} \langle E \rangle = \frac{2}{3} \int E^{3/2} f(E)dE \; / \; \int E^{1/2} f(E)dE.$$

A T_{eff} of $\sim$ 3.2 keV has been obtained at 2.8 MW at $\bar{n}_e = 3.5 \times 10^{13}$ cm^{-3}. As can be seen in Fig. 11, the increase in T_{eff} has remained roughly linear with increasing absorbed ICRF power in the absence of m = 2 activity. The second harmonic heated discharges represented in Fig. 11 were not optimized to produce the best ion heating efficiencies. Caution should be used in comparing T_{eff} with other measurements of T_i. If, for example, a similar T_{eff} is calculated for the H minority case, the ratio of the effective temperature to the bulk deuteron temperature is typically 1.2 - 1.5, due to the proton tail contributions to the ion energy.

In general, the minority ^{3}He and H experiments show clear evidence of electron heating at low minority concentrations consistent with expected tail ion-electron coupling. In the second harmonic regime, no significant electron heating has been observed perhaps owing to the degraded τ_{Ee} at the required

low operating toroidal fields (~ 1.4 T) and a large associated density rise. Up to 1 eV/kW of electron heating at $\bar{n}_e \sim 3 \times 10^{13}$ cm^{-3} has been observed in the best minority H heating case with 600 kW on ICRF delivered. Similar heating has been observed with the ^{3}He case as described earlier.

Some initial low q, high β auxiliary heating experiments have been run on PLT with the neutral beams plus ICRF. An experiment was performed with a deuterium plasma at 1.7 T with 1.3 MW from the 25 MHz system and 1.8 MW of deuterium beams. This combined beams plus minority hydrogen heating experiment produced an electron energy of ~ 50 kJ corresponding to a β_e value of 0.7% (Fig. 13). The discharge has been found to be reproducible, generally giving kinetic β_i [from doppler broadening measurements of the T_i profile (Suckewer 1981)] and $\beta_e \gtrsim 0.6\%$ for comparable power levels. An energy analysis with T_e from Thomson scattering and T_i from doppler broadening measurements with a conservative beam contribution to β_T (ignoring any direct beam - RF interaction) yields $\beta_T \sim 1.6\%$. Diamagnetic and equilibrium β measurements indicate a β_T value of 1.8 - 2.2% (Hosea 1982). The ability to quote more exact measurements of β is hampered at present by the interpretation of the magnetic signals.

Several other interesting discharges in the low q, high β regime include a beam heated discharge (1.8 MW D°) at 1.4 T with $q_{cyl} \leq 1.6$. Toroidal betas values from energy analysis (based on TVTS and passive charge exchange) of 1% have been obtained with 3 beam operation alone (1.7 MW absorbed), which is close to the PDX results for similar conditions and powers. In the near future, the available power from beams plus ICRF should allow exploration of considerably higher beta regimes.

4. LOWER HYBRID RESULTS

The PLT lower hybrid system (800 MHz) has been operated in a density range ($1x10^{13}$ cm^{-3} < $\bar{n}_e$ < $3x10^{13}$ cm^{-3}) to study bulk plasma heating, and in a low density range (< 10^{13} cm^{-3}) to study current drive (Stevens 1982). A schematic of PLT and the lower hybrid system is shown in Fig. 14. The coupler consists of six adjacent waveguides 3.5 cm x 22 cm each, with E parallel to the toroidal magnetic field. Several improvements were added to the coupler in September of 1981, which have increased the power from 35 to 125 kW/guide. These changes were:

1) The inside surfaces were coated with carbon to reduce secondary emission and thus multipacting (Ruzic 1982).
2) The ends of the waveguides facing the plasma were rounded.
3) The primary limiters were moved from near the coupler to a location 80° toroidally away, in an effort to reduce neutral gas near the coupler.
4) An additional gas puff located far from the LH coupler was used.

Although it is not clear which of these improvements was the most important, the power in each waveguide was increased to 1.6 kW/cm^2 without breakdown or arcing.

Heating experiments in the higher density range ($1.7 > \omega/\omega_{\ell h} > 1.0$) have shown an enhancement of 2.5 MeV neutron emission of roughly 2-1/2 orders of magnitude. The emission decays with a 20 msec time constant after the lower hybrid is turned off. An energetic ion tail is also observed on the perpendicularly and horizontally scanning charge exchange analyzers (Fig. 15). This tail is also observed by the spectral broadening of 3 MeV protons from the d(d,p)t reaction (Chrien 1981). Active charge exchange

measurements indicate that the perpendicular component of this tail is not located in the center of the plasma. Although the horizontally scanning charge exchange analyzer shows some bulk heating, preliminary results show heating to be inefficient.

Lower hybrid current drive studies on PLT at densities below $\sim 7 \times 10^{12}$ cm^{-3} have demonstrated the ability to sustain large plasma currents with RF alone (Jobes 1982). The experiments are performed by either holding $dI_{OH}/dt = 0$ or $I_{OH} = 0$ for the duration of the LH, where I_{OH} is the primary current in ohmic heating coils. During a typical current drive experiment ($\bar{n}_e \simeq 3 \times 10^{12}$ cm^{-3}, $P_{LH} = 80$ kW) the electron and ion temperatures are held fairly constant [$T_e(o) \sim 1.0$ keV, $T_i(o) \sim 400$ eV]. Figure 16 shows a current drive discharge where the plasma current was held constant by the lower hybrid for 3.5 seconds with $dI_{OH}/dt = 0$, $\bar{n}_e = 3 \times 10^{12}$ cm^{-3}, $P_{LH} = 75$ kW, and $I_p = 160$ kA. The length of the current pulse was limited by equipment safety considerations rather than by any physics or lower hybrid power handling limits. For shorter times (0.3 sec) current levels up to 400 kA have been driven by the RF. The current drive efficiency peaks with an adjacent waveguide phasing of 60° to 90° (corresponding to a traveling wave in the electron drift direction), while the opposite phasing of -60° to -90° produces little or no effect. With the magnetic fields and plasma current reversed, the waveguide phasing must be reversed to yield the same results.

In addition to the waveguide phasing, the current drive efficiency is also dependent on the plasma current, density and lower hybrid power. For $\bar{n}_e < 6 \times 10^{12}$ cm^{-3}, we find that $\bar{n}_e I_p/P_{LH} \simeq 6 \times 10^{12}$ A/W cm^3. The current drive effect disappears above 10^{13} cm^{-3}.

The main current carrier in the plasma with lower hybrid current drive appears to be a core of fast electrons in the center of the plasma. Evidence

for these electrons is seen in both the electron cyclotron emission and the X-ray radiation. The hard X-ray spectrum (20 - 500 keV) measured vertically through the center of the plasma shows the formation of an enhanced X-ray distribution during lower hybrid current drive (Fig. 17). Horizontal X-ray scans across the body of the plasma column indicate that the X-ray emission is mostly from the inner 15 cm of the plasma. The central X-ray distribution can be modeled by assuming that a 15 cm core of electrons (~ 4% of the central electrons) is flowing in the electron drift direction with a 150 keV, relativistic, half Maxwellian velocity distribution. Experiments are being prepared to measure the photon energy distribution at other angles.

Above densities of about 7×10^{12} cm^{-3}, the plasma current can no longer be maintained at a constant level (Fig. 18). Above densities of $0.9 - 1 \times 10^{13}$ cm^{-3}, the current drive effect completely disappears. The inability to drive current at higher densities appears to correlate with several things, including the onset of RF decay wave spectra, a sharp cooling of the electron body temperature, and a theoretically predicted decrease in the $n_{\parallel}$ spectrum of the RF. These and other possible explanations for the current drive density limit are under investigation.

5. CONCLUSIONS

In summary, on PDX, ion temperatures of ~ 6 keV have been obtained with approximately perpendicular injection. Ion heating as well as plasma stored energy improve with current, whereas no change in stored energy is seen with changes in toroidal field ($2.4\ T > B_T > 1.0\ T$). Beta values of 3.2% have been achieved with β rising with increasing absorbed beam power. However, MHD behavior observed at high β appears to result in significant losses of perpendicular bulk and suprathermal ions.

On PLT, ICRF heating in both minority and second harmonic modes have continued to higher power levels. The 3 MW level has been reached at 42 MHZ in the second harmonic H regime. Experiments with ICRF plus beam heating have produced substantial plasmas betas ($\gtrsim$ 1.6%) at relatively high magnetic fields (1.7 T).

The lower hybrid experiments on PLT have demonstrated current drive at plasma densities $< 1 \times 10^{13}$ cm^{-3}, and have been used to maintain plasma temperatures and drive plasma currents of $\sim$ 400 kA for 0.3 seconds and 160 kA for up to 3.5 seconds in the absence of any applied inductive fields.

ACKNOWLEDGMENTS

The authors would like to thank Dr. H.P. Furth, Dr. P.H. Rutherford and Dr. Dale Meade for their continuing support and encouragement. We would also like to thank our many colleagues in the laboratory, who are not part of the PLT and PDX groups, but whose contributions have made this work possible. This work was supported by U.S. DOE Contract No. DE-AC02-76-CHO-3073.

REFERENCES

Bell, M. et al. (1981) to be published in Controlled Fusion and Plasma Physics, Proc. of the X European Conference (Moscow 1981) Volume 2.

Chang, C.S. and Hinton, F.L. (1982) GA-A16678, General Atomic.

Cohen, R.E. et al. (1981) Phys. Rev. Lett. **46**, 535.

Dunlap, J.L. (1982) Phys. Rev. Lett **48**, 538.

Goldston, R.J. et al. (1981) Heating in Toroidal Plasmas Proc. 2nd Joint Grenoble-Varenna Inter. Symp. Vol. II, CEC, Brussels (1981) 711.

Goldston, R.J. et al. (1982) Third Joint Varenna-Grenoble Inter. Symp. on Heating in Toroidal Plasmas.

Hawryluk, R. et al. (1982) PPPL-1882, Princeton University.

Hosea, J. et al. (1979) Presented at the Course and Workshop on Physics of Plasmas Close to Thermonuclear Conditions, Varenna, Italy, August 1979.

Hosea, J., et al. (1982) Third Joint Varenna-Grenoble Inter. Symp. on Heating in Toroidal Plasmas.

Jobes, F.C. et al. (1982) Presented at the Symposium on New Ideas and Unconventional Treads in Magnetic Confinement, Goteborg, Sweden.

Lomas, P.J. et al. (1981) Proc. 10th European Conf. on Controlled Fusion and Plasma Physics, Moscow (Sept. 1981) Vol. I, Paper A-1.

Porkolab, M. et al. (1977) Phys. Rev. Lett **38**, 230.

Ruzic, D., et al. (1982) PPPL-1874, Princeton Univ.

(PPPL 1981) Princeton University Plasma Physics Lab Annual Report.

Stevens, J.E. et al. (1982) Third Joint Varenna-Grenoble Inter. Symp. on Heating in Toroidal Plasmas.

Stodiek, W. et al. (1980) Proc. 8th Inter. Conf. Plasma Physics and Controlled Nuclear Fusion Research, (IAEA, Vienna 1981), Vol. I, 9.

Suckewer, S. et al. (1980) Phys. Lett. **80A**, 259.

Suckewer, S. et al. (1981) Nucl. Fusion **21**, 981.

Swain, D.W et al. (1981) Nucl. Fusion **21**, 1409.

Vehara, et al. (1982) Third Joint Varenna-Grenoble Inter. Symp. on Heating in Toroidal Plasmas.

Yamamoto, S. et al. (1981) Nucl. Fusion **21**, 993.

FIGURE CAPTIONS

Fig. 1 Central ion temperature versus time for a hydrogen plasma with deuterium injection with I_p = 500 kA, B_t = 2.24 T, and $\bar{n}_e$ = 3.8 x 10^{13} cm^{-3}. The active charge exchange point taken during injection is ~ 6 cm off axis because of the Shafranov shift during heating. The active charge exchange point taken during the ohmic phase is ~ 3 cm off axis.

Fig. 2 Scaling of the passively measured ion temperature as a function of absorbed power divided by line average density in PDX. The density is in the range 2 - 4 x 10^{13} cm^{-3}.

Fig. 3 Increase in the magnetically determined $\ell_i/2 + \beta_p$ with absorbed beam power for several plasma currents at a toroidal field of 2.2 T in PDX.

Fig. 4 The increase in β_T in PDX as measured from the equilibrium field. The scan was done at a toroidal field of 1.0 T, I_p = 300 kA, using a circular plasma with $D \rightarrow H^+$ and R/a = 143/40 cm.

Fig. 5 The energy content from equilibrium magnetic measurements is compared for 2.2 T and 1.0 T discharges. The data are restricted to PDX circular discharges with I_p = 300 kA, $D^o \rightarrow H^+$ and R_o = 143 cm.

Fig. 6 MHD activity are observed during high power neutral injection on PDX by the ultra soft X-ray wave detector array and by a Mirnov coil located just inside the outside vacuum wall.

Fig. 7 The correlation of the MHD activity of high β PDX discharges as observed on the Mirnov coils, the soft X-ray wave detector array, the charge exchange flux and the neutron flux.

Fig. 8 The charge exchange flux during the MHD activity of high β PDX discharges has been observed by the horizontally scanning analyzer at two different tangency radii. The ratio of the fluxes is plotted as a function of energy. The flux is more strongly peaked in the perpendicular direction when this ratio is low. The data points plotted with the small arrows indicate that the data point is plotted at the maximum value for that point and is probably lower.

Fig. 9 The neutron flux and the deduced deuterium temperature for a ^3He minority deuterium plasma with 1.2 MW delivered to the PLT plasma from 400 to 575 msec (f = 25 MHz, $\bar{n}_e = 3.2 \times 10^{13}$ cm^{-3}, $B_T = 2.5$ T).

Fig. 10 Thomson scattering measurements of electron heating from a ^3He minority deuterium plasma with 1.5 MW delivered. The density rose from 3 to 3.8 x 10^{13} cm^{-3} during the heating.

Fig. 11 The increase in passively measured ion temperature as a function of absorbed ICRF power divided by line average density in PLT. The lines and open data points refer to the minority ^3He and H heating cases. The solid points refer to second harmonic heating cases. T_{eff} is defined in the text.

Fig. 12 The charge exchange energy distribution function taken during second harmonic heating of a hydrogen plasma in PLT with 2.9 MW of absorbed power at 42 MHz with $\bar{n}_e \sim 4 \times 10^{13}$, $I_p \sim 400$ kA, and $B_t = 1.4$ T. The solid curve is the fit used to find T_{eff} as described in the text.

Fig. 13 Electron temperature and density profiles from the PLT Thomson scattering ~ 50 kJ of electron energy content which was achieved with 2.0 MW of D° beams and 1.3 MW of minority H heating ($q_{cyl} = 2.1$).

Fig. 14 Schematic of PLT and the lower hybrid system.

Fig. 15 Perpendicular charge exchange spectrum during the application of 350 kW of lower hybrid power with $\bar{n}_e = 1.9 \times 10^{13}$ cm^{-3}. R_{tan} is the distance of closest approach of the sightline to the PLT axis of symmetry.

Fig. 16 The current and density from a PLT lower hybrid current drive experiment where the lower hybrid was applied for 3.5 seconds with $dI_{OH}/dt = 0$.

Fig. 17 PLT hard X-ray spectrum with and without lower hybrid at $\bar{n}_e = 6 \times 10^{12}$ cm^{-3}. The inset shows the time evolution of the plasma X rays and the limiter X rays (inverted scale). The RF power is 200 kW and is on from 300 to 700 msec.

Fig. 18 dI_p/dt versus density for several power levels showing that the density dependence of the current drive on PLT encounters a cutoff at roughly $\bar{n}_e = 8 \times 10^{12}$ cm^{-3}.

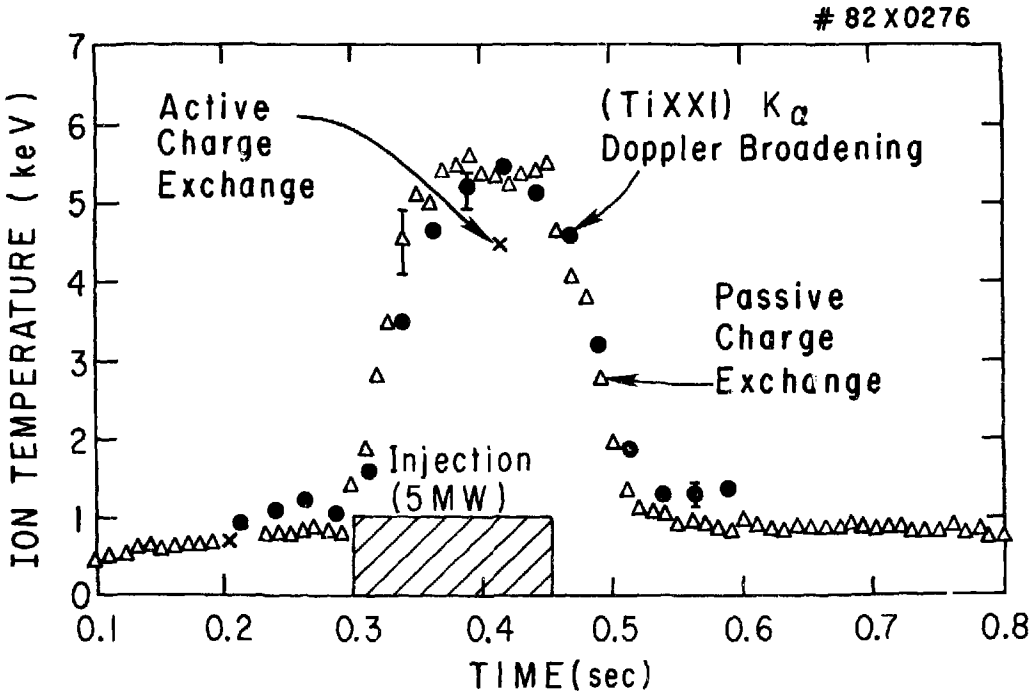
82X0276
ION TEMPERATURE (keV)
TIME(sec)
Active Charge Exchange
(TiXXI) Kα Doppler Broadening
Passive Charge Exchange
Injection (5MW)
0
1
2
3
4
5
6
7
0.1
0.2
0.3
0.4
0.5
0.6
0.7
0.8

FIG. 1

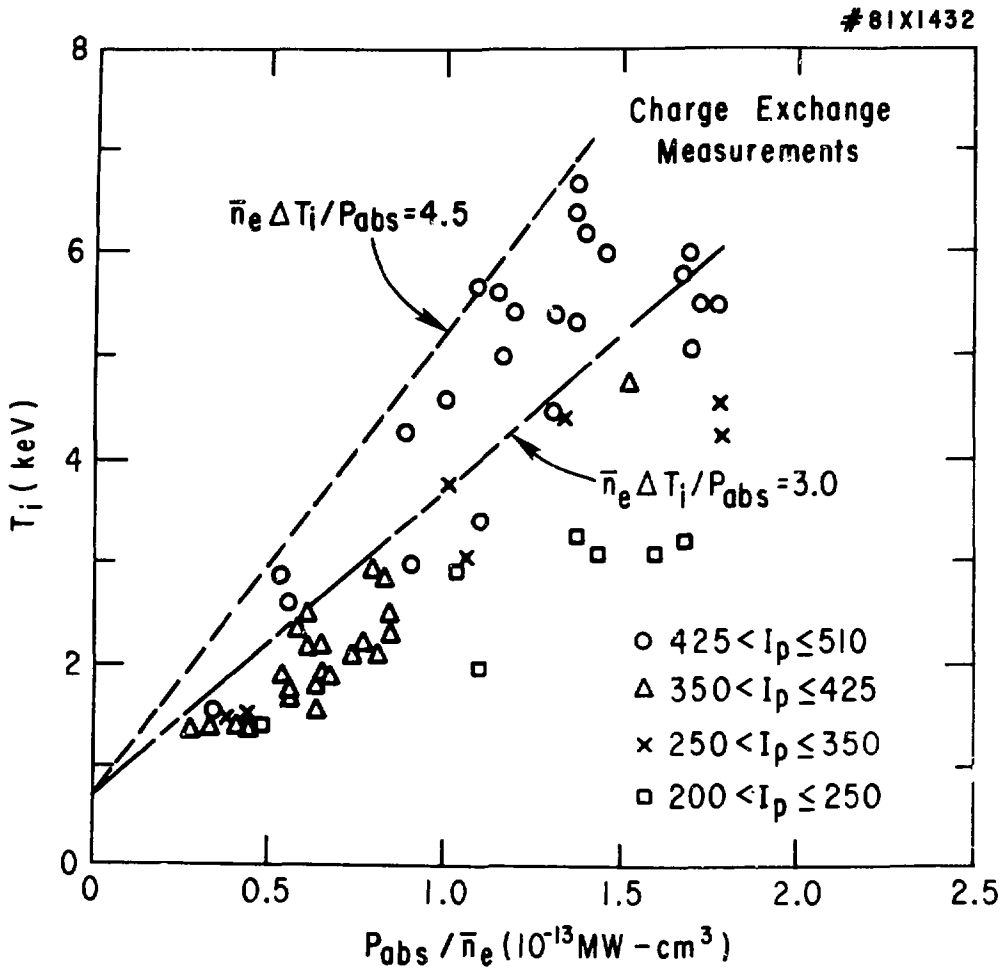
#81X1432
Charge Exchange
Measurements
$\bar{n}_e \Delta T_i / P_{abs} = 4.5$
$\bar{n}_e \Delta T_i / P_{abs} = 3.0$
$425 < I_p \leq 510$
$350 < I_p \leq 425$
$250 < I_p \leq 350$
$200 < I_p \leq 250$
T_i (keV)
$P_{abs} / \bar{n}_e$ (10^{-13}MW - cm^3)
0
2
4
6
8
0
0.5
1.0
1.5
2.0
2.5

FIG. 2

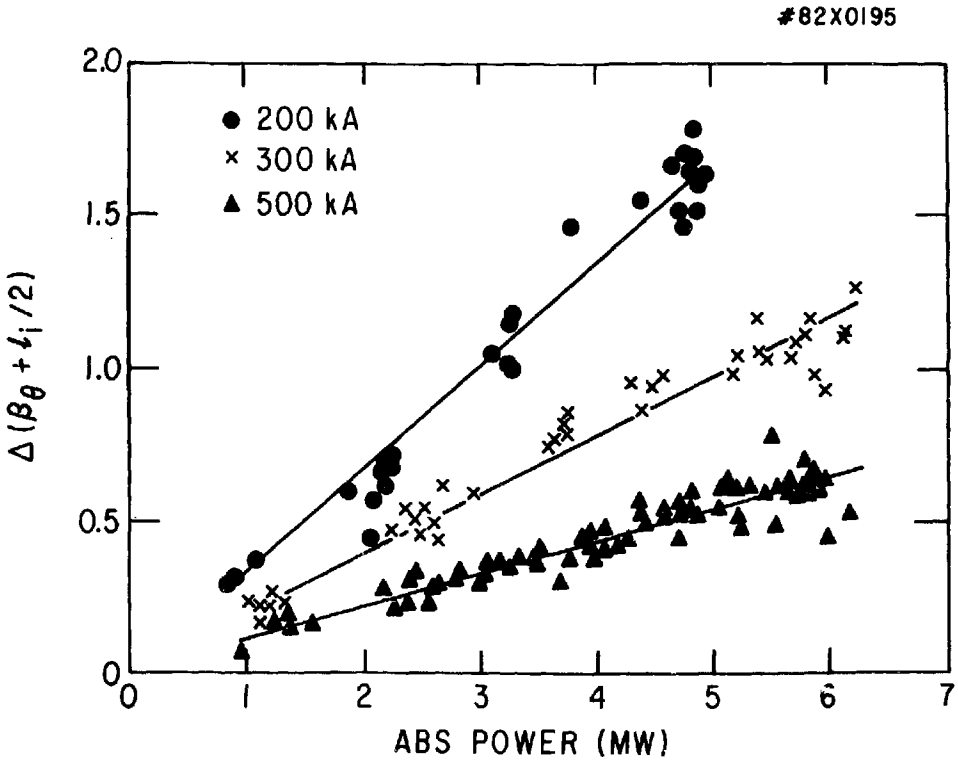
#82X0195
2.0
1.5
1.0
0.5
0
0
1
2
3
4
5
6
7
200 kA
300 kA
500 kA
$\Delta(\beta_\theta + \ell_i/2)$
ABS POWER (MW)

FIG. 3

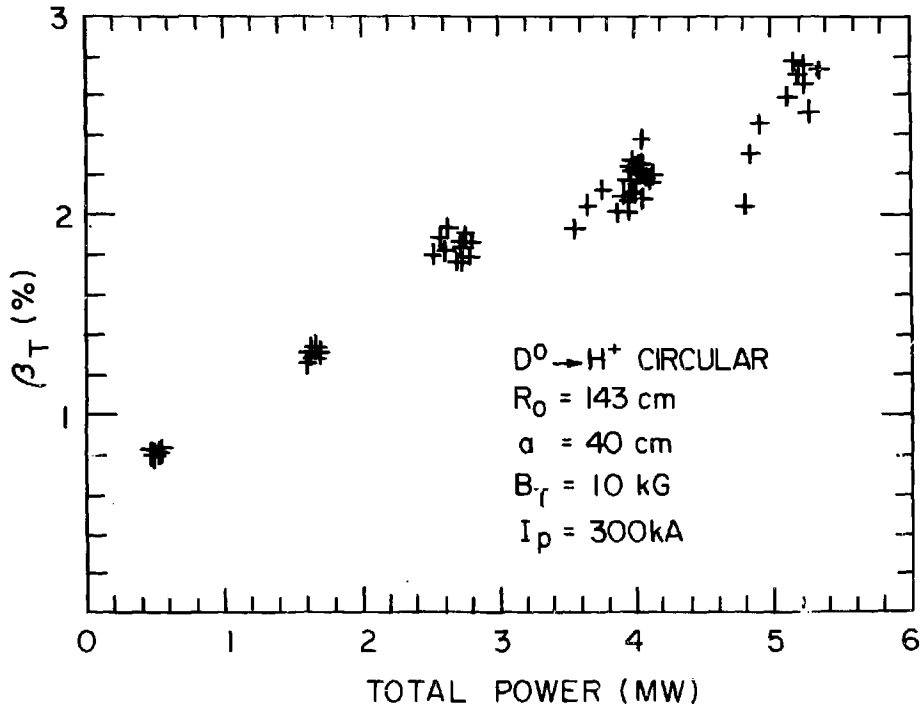
3
2
1
β_T (%)
$D^0 \rightarrow H^+$ CIRCULAR
R_0 = 143 cm
a = 40 cm
B_f = 10 kG
I_p = 300kA
0
1
2
3
4
5
6
TOTAL POWER (MW)

FIG. 4

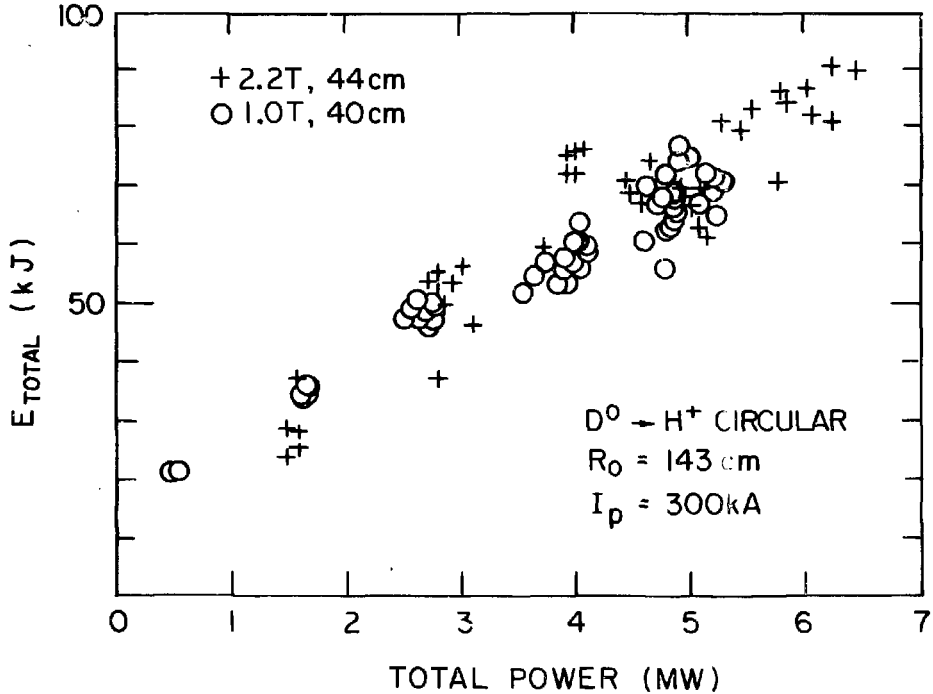
100
50
+ 2.2T, 44cm
O 1.0T, 40cm
D⁰ → H⁺ CIRCULAR
R₀ = 143 cm
Iₚ = 300kA
E TOTAL (kJ)
0
1
2
3
4
5
6
7
TOTAL POWER (MW)

FIG. 5

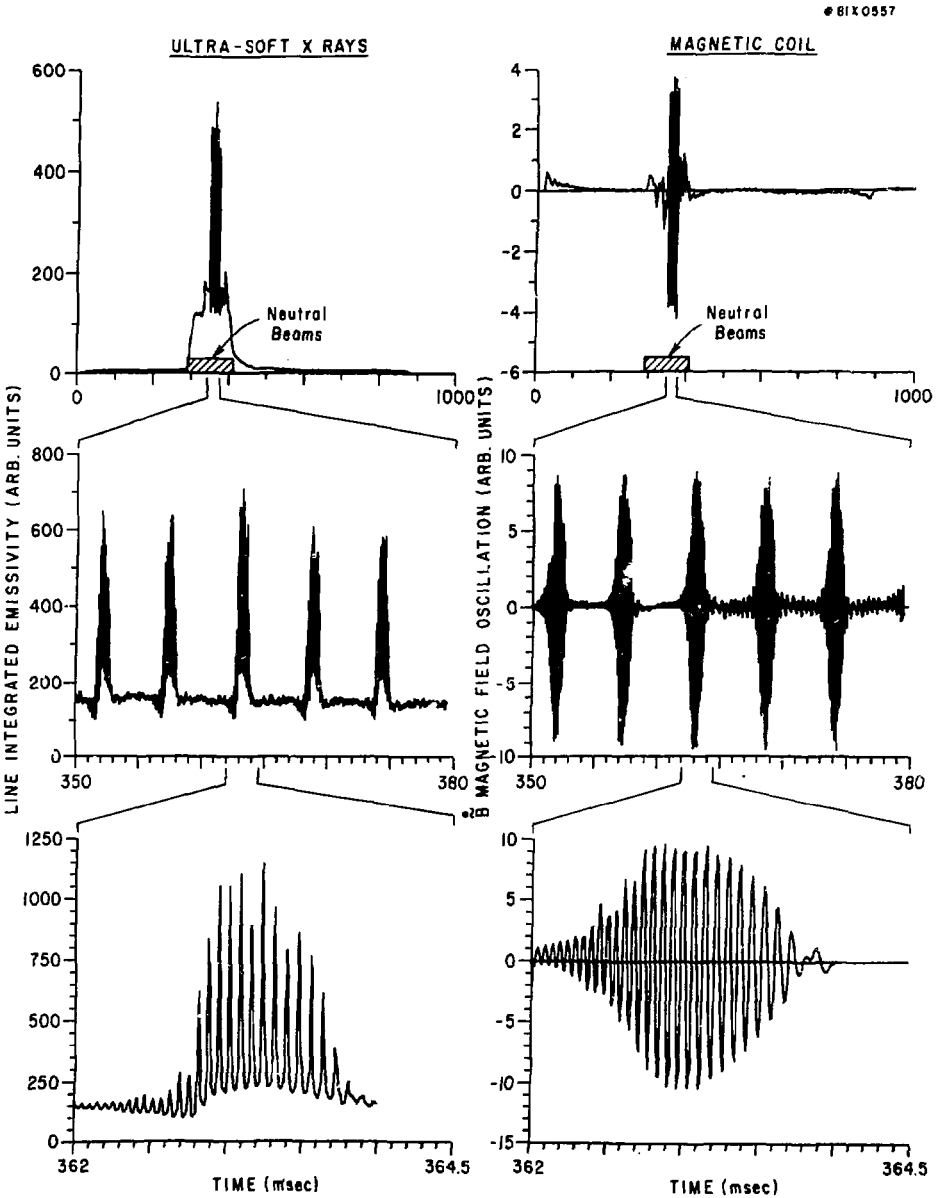
#81X0557
ULTRA-SOFT X RAYS
MAGNETIC COIL
Neutral Beams
Neutral Beams
LINE INTEGRATED EMISSIVITY (ARB. UNITS)
B MAGNETIC FIELD OSCILLATION (ARB. UNITS)
TIME (msec)
TIME (msec)

FIG. 6

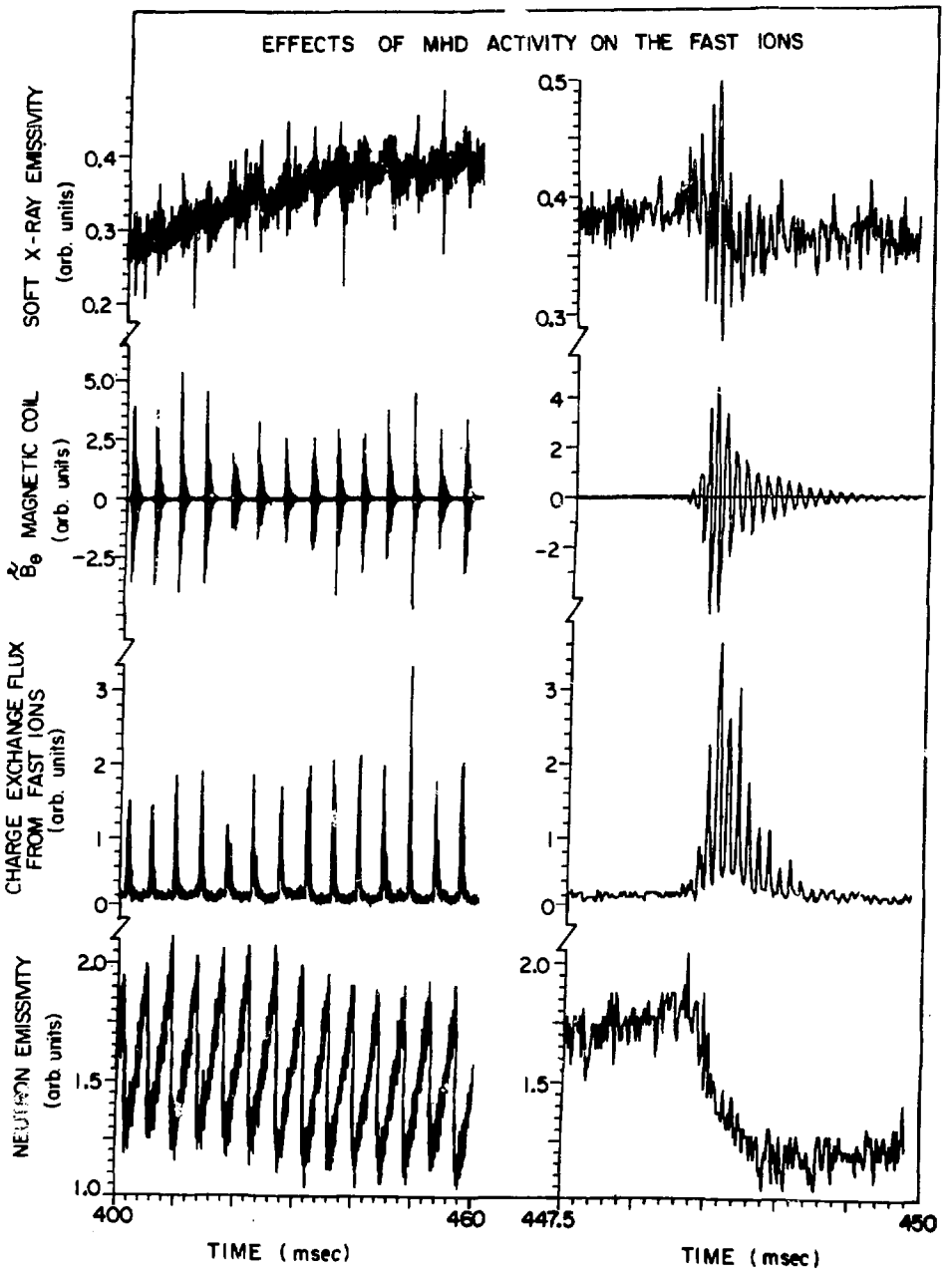
EFFECTS OF MHD ACTIVITY ON THE FAST IONS
SOFT X-RAY EMISSIVITY (arb. units)
MAGNETIC COIL $\tilde{B}_\theta$ (arb. units)
CHARGE EXCHANGE FLUX FROM FAST IONS (arb. units)
NEUTRON EMISSIVITY (arb. units)
TIME (msec)
TIME (msec)

FIG. 7

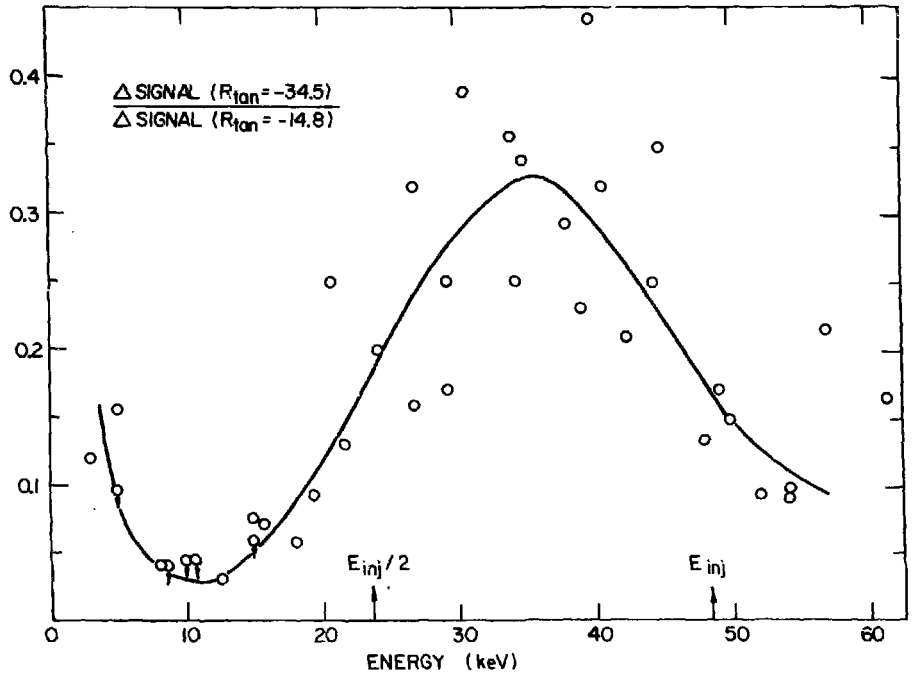
Δ SIGNAL (R_{tan} = -34.5)
Δ SIGNAL (R_{tan} = -14.8)
0.4
0.3
0.2
0.1
0
10
20
30
40
50
60
$E_{inj}/2$
E_{inj}
ENERGY (keV)

FIG. 8

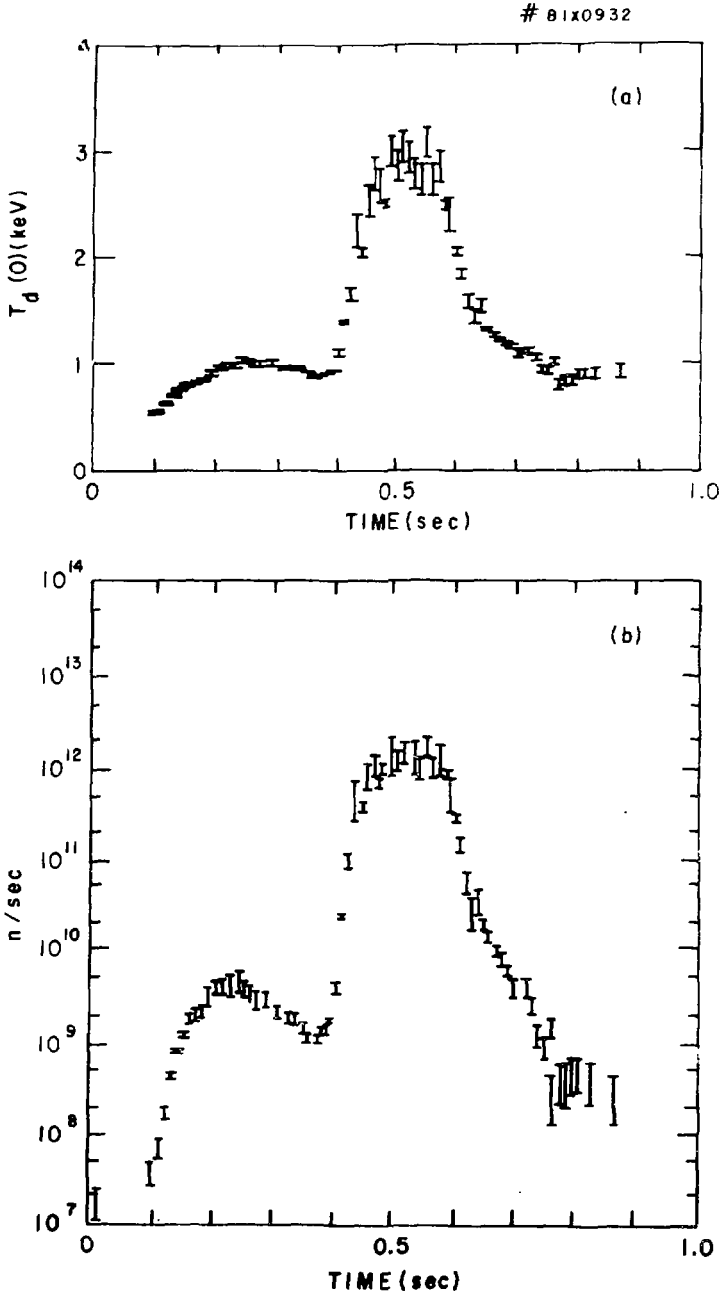

FIG. 9

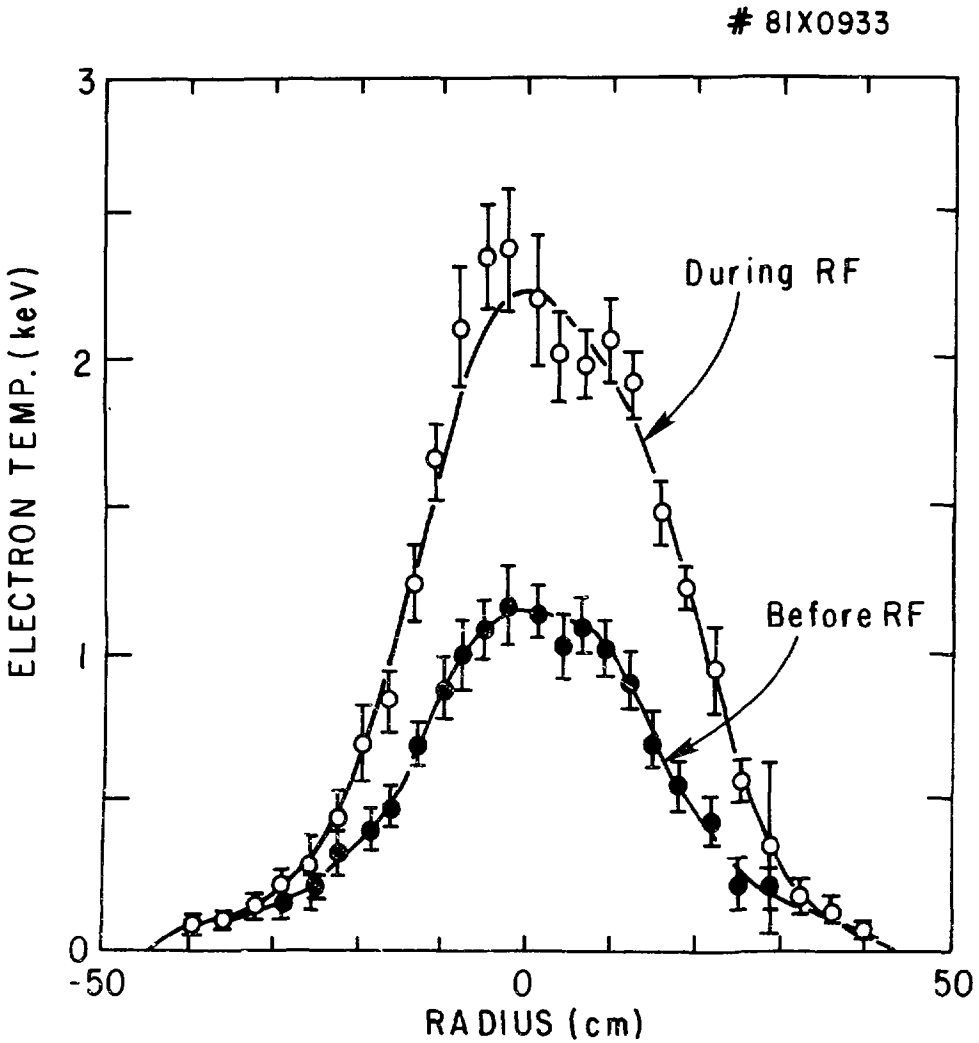
81X0933
ELECTRON TEMP. (keV)
3
2
1
0
-50
0
50
RADIUS (cm)
During RF
Before RF

FIG. 10

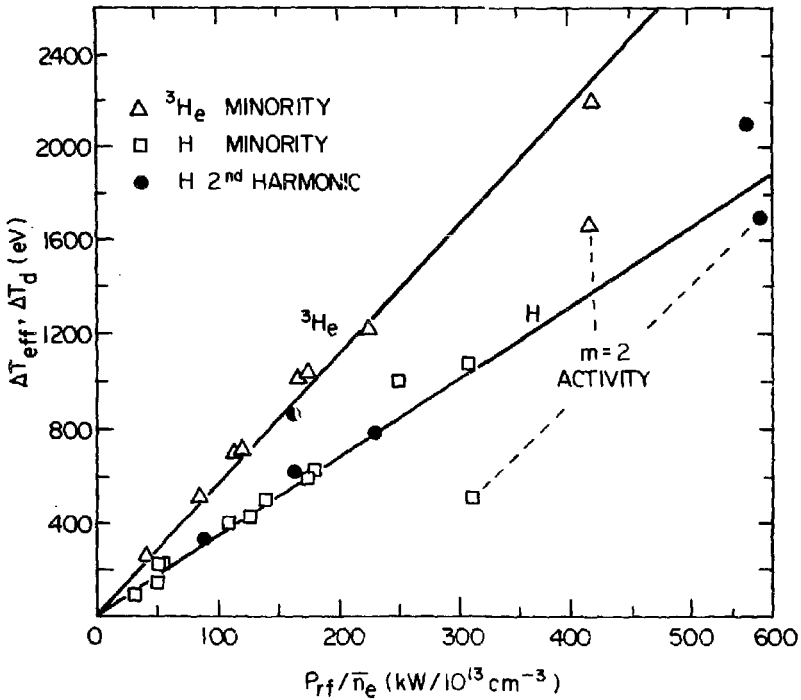
2400
2000
1600
1200
800
400
0
100
200
300
400
500
600
ΔT_{eff}, ΔT_d (eV)
$P_{rf}/\bar{n}_e$ (kW/10^{13} cm^{-3})
△ ^{3}He MINORITY
□ H MINORITY
● H 2nd HARMONIC
^{3}He
H
m = 2
ACTIVITY

FIG. 11

#82X0165

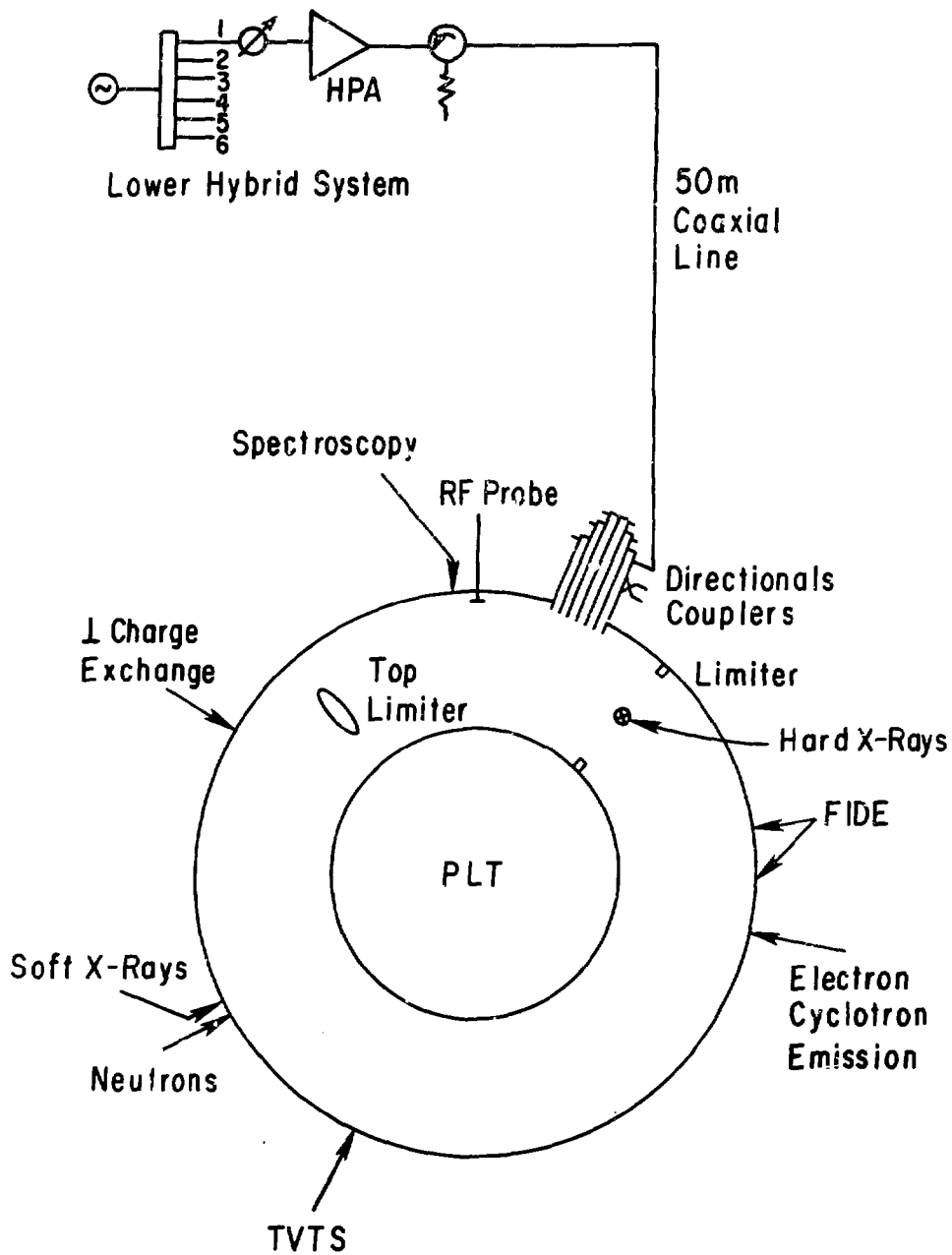

Fig. 14

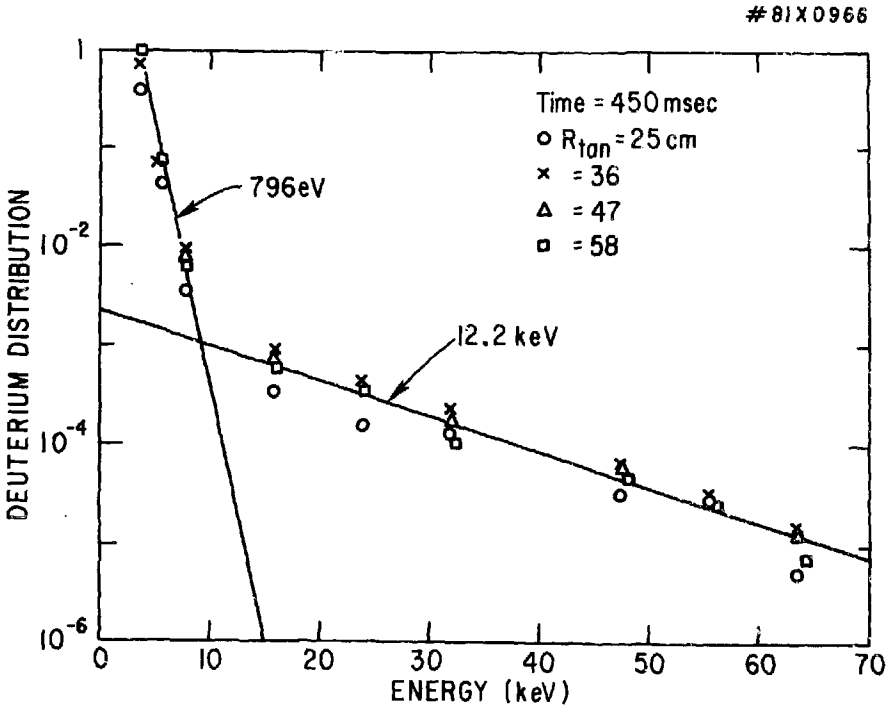
#81X0966
Time = 450 msec
o R_{tan} = 25 cm
× = 36
Δ = 47
□ = 58
796eV
12.2 keV
DEUTERIUM DISTRIBUTION
1
10^{-2}
10^{-4}
10^{-6}
0
10
20
30
40
50
60
70
ENERGY (keV)

FIG. 15

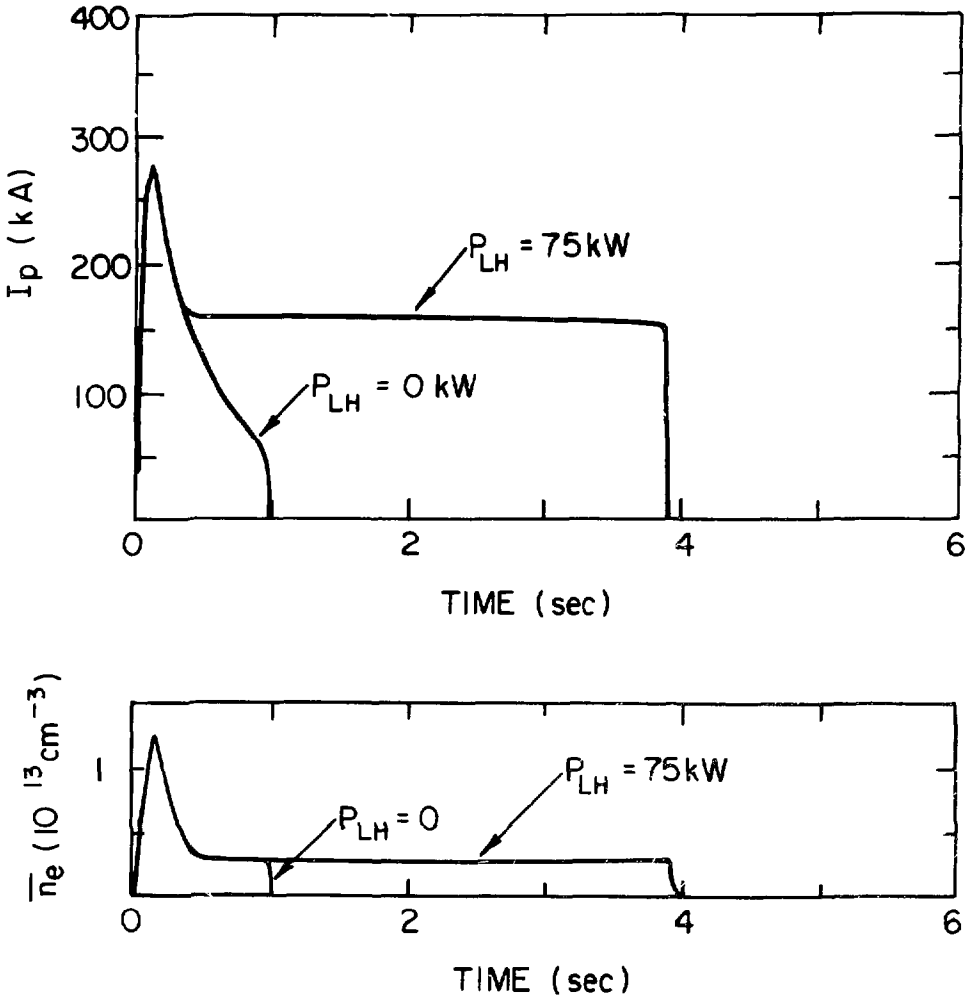
400
300
200
100
I_p (kA)
P_{LH} = 75kW
P_{LH} = 0 kW
0
2
4
6
TIME (sec)
$\overline{n_e}$ (10^{13} cm^{-3})
1
P_{LH} = 75kW
P_{LH} = 0
0
2
4
6
TIME (sec)

FIG. 16

#82X0054

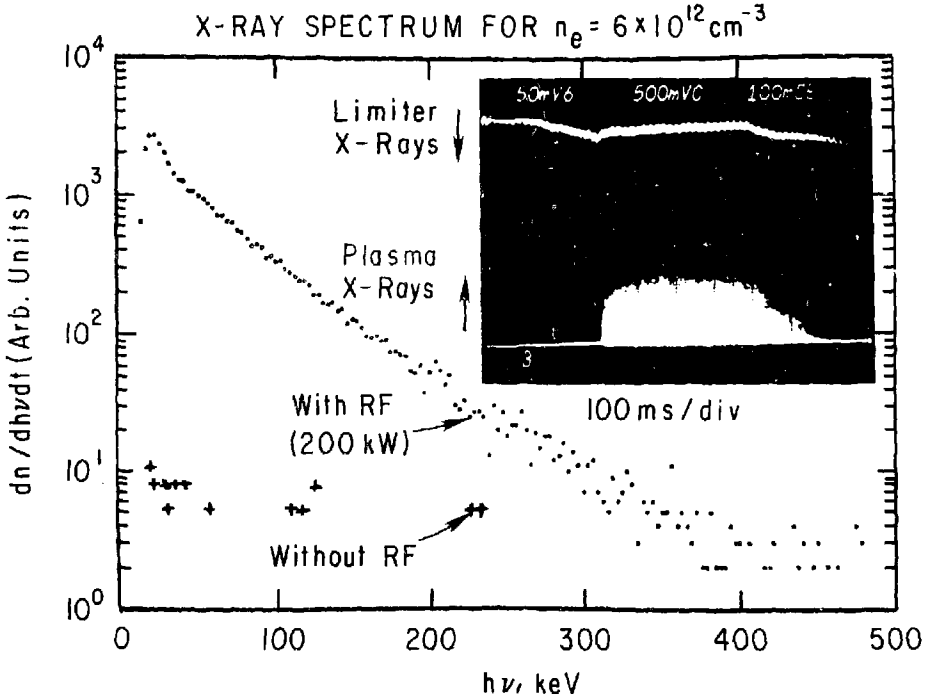

FIG. 17

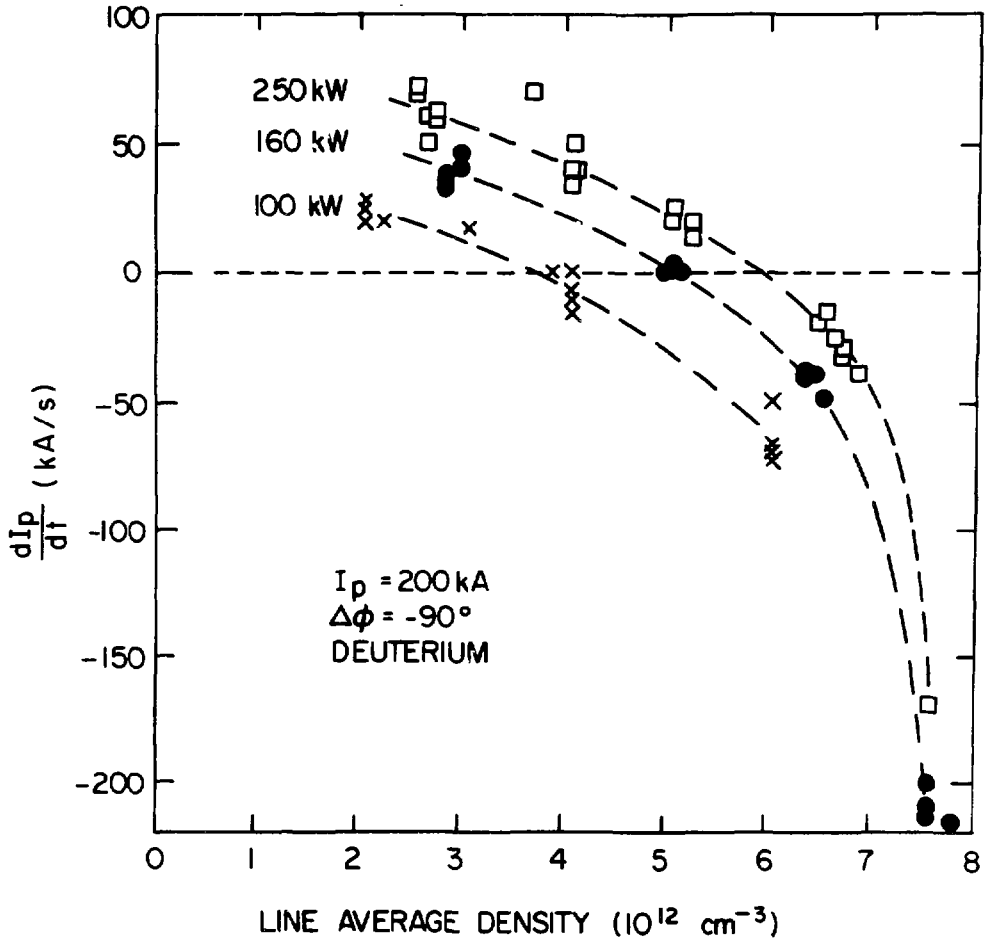
250 kW
160 kW
100 kW
I_p = 200 kA
$\Delta\phi$ = -90°
DEUTERIUM
$\frac{dI_p}{dt}$ (kA/s)
LINE AVERAGE DENSITY (10^{12} cm^{-3})
100
50
0
-50
-100
-150
-200
0
1
2
3
4
5
6
7
8

FIG. 18

EXTERNAL DISTRIBUTION IN ADDITION TO TIC UC-20

Plasma Res Lab, Austra Nat'l Univ, AUSTRALIA
Dr. Frank J. Paoloni, Univ of Wollongong, AUSTRALIA
Prof. I.R. Jones, Flinders Univ., AUSTRALIA
Prof. M.H. Brennan, Univ Sydney, AUSTRALIA
Prof. F. Cap, Inst Theo Phys, AUSTRIA
Prof. Frank Verheest, Inst theoretische, BELGIUM
Dr. D. Palumbo, Dg XII Fusion Prog, BELGIUM
Ecole Royale Militaire, Lab de Phys Plasmas, BELGIUM
Dr. P.H. Sakanaka, Univ Estadual, BRAZIL
Dr. C.R. James, Univ of Alberta, CANADA
Prof. J. Teichmann, Univ of Montreal, CANADA
Dr. H.M. Skarsgard, Univ of Saskatchewan, CANADA
Prof. S.R. Sreenivasan, University of Calgary, CANADA
Prof. Tudor W. Johnston, INRS-Energie, CANADA
Dr. Hannes Barnard, Univ British Columbia, CANADA
Dr. M.P. Bachynski, MPB Technologies, Inc., CANADA
Zhengwu Li, SW Inst Physics, CHINA
Library, Tsing Hua University, CHINA
Librarian, Institute of Physics, CHINA
Inst Plasma Phys, SW Inst Physics, CHINA
Dr. Peter Lukac, Komenskeho Univ, CZECHOSLOVAKIA
The Librarian, Culham Laboratory, ENGLAND
Prof. Schatzman, Observatoire de Nice, FRANCE
J. Radet, CEN-BP6, FRANCE
AM Dupas Library, AM Dupas Library, FRANCE
Dr. Tom Mual, Academy Bibliographic, HONG KONG
Preprint Library, Cent Res Inst Phys, HUNGARY
Dr. A.K. Sundaram, Physical Research Lab, INDIA
Dr. S.K. Trehan, Panjab University, INDIA
Dr. Indra, Mohan Lal Das, Banaras Hindu Univ, INDIA
Dr. L.K. Chavda, South Gujarat Univ, INDIA
Dr. R.K. Chhajlani, Var Ruchi Marg, INDIA
B. Buti, Physical Research Lab, INDIA
Dr. Phillip Rosenau, Israel Inst Tech, ISRAEL
Prof. S. Cuperman, Tel Aviv University, ISRAEL
Prof. G. Rostagni, Univ Di Padova, ITALY
Librarian, Int'l Ctr Theo Phys, ITALY
Miss Clelia De Palo, Assoc EURATOM-CNEN, ITALY
Biblioteca, del CNR EURATOM, ITALY
Dr. H. Yamato, Toshiba Res & Dev, JAPAN
Prof. M. Yoshikawa, JAERI, Tokai Res Est, JAPAN
Prof. T. Uchida, University of Tokyo, JAPAN
Research Info Center, Nagoya University, JAPAN
Prof. Kyoji Nishikawa, Univ of Hiroshima, JAPAN
Sigeru Mori, JAERI, JAPAN
Library, Kyoto University, JAPAN
Prof. Ichiro Kawakami, Nihon Univ, JAPAN
Prof. Satoshi Itoh, Kyushu University, JAPAN
Tech Info Division, Korea Atomic Energy, KOREA
Dr. R. England, Ciudad Universitaria, MEXICO
Bibliotheek, Fom-Inst Voor Plasma, NETHERLANDS
Prof. B.S. Liley, University of Waikato, NEW ZEALAND
Dr. Suresh C. Sharma, Univ of Calabar, NIGERIA
Prof. J.A.C. Cabral, Inst Superior Tech, PORTUGAL
Dr. Octavian Petrus, ALI CUZA University, ROMANIA
Dr. R. Jones, Nat'l Univ Singapore, SINGAPORE
Prof. M.A. Hellberg, University of Natal, SO AFRICA
Dr. Johan de Villiers, Atomic Energy Bd, SO AFRICA
Dr. J.A. Tagle, JEN, SPAIN
Prof. Hans Wilhelmson, Chalmers Univ Tech, SWEDEN
Dr. Lennart Stenflo, University of UMEA, SWEDEN
Library, Royal Inst Tech, SWEDEN
Dr. Erik T. Karlson, Uppsala Universitet, SWEDEN
Centre de Recherchesen, Ecole Polytech Fed, SWITZERLAND
Dr. W.L. Weise, Nat'l Bur Stand, USA
Dr. W.M. Stacey, Georg Inst Tech, USA
Dr. S.T. Wu, Univ Alabama, USA
Mr. Norman L. Oleson, Univ S Florida, USA
Dr. Benjamin Ma, Iowa State Univ, USA
Magne Kristiansen, Texas Tech Univ, USA
Dr. Raymond Askew, Auburn Univ, USA
Dr. V.T. Tolok, Kharkov Phys Tech Ins, USSR
Dr. D.D. Ryutov, Siberian Acad Sci, USSR
Dr. M.S. Rabinovich, Lebedev Physical Inst, USSR
Dr. G.A. Eliseev, Kurchatov Institute, USSR
Dr. V.A. Glukhikh, Inst Electro-Physical, USSR
Prof. T.J. Boyd, Univ College N Wales, WALES
Dr. K. Schindler, Ruhr Universitat, W. GERMANY
Nuclear Res Estab, Julich Ltd, W. GERMANY
Librarian, Max-Planck Institut, W. GERMANY
Dr. H.J. Kaeppler, University Stuttgart, W. GERMANY
Bibliothek, Inst Plasmaforschung, W. GERMANY